SCIENTIFIC REPORTS

OPEN

SUBJECT AREAS:
COMPUTATIONAL MODELS
MOLECULAR MODELLING

Received
9 August 2013

Accepted
13 January 2014

Published
3 February 2014

Correspondence and requests for materials should be addressed to M.R. (marasri.rue@kmutt.ac.th)

Defining the membrane disruption mechanism of kalata B1 via coarse-grained molecular dynamics simulations

Wanapinun Nawae[1], Supa Hannongbua[2] & Marasri Ruengjitchatchawalya[3,4]

[1]Biological Engineering Program, King Mongkut's University of Technology Thonburi, 126 Pracha Uthit Rd., Bang Mod, Thung Khru, Bangkok, Thailand, 10140, [2]Department of Chemistry, Kasetsart University, 50 Phaholyothin Rd., Ladyao Chatuchak, Bangkok, Thailand, 10900, [3]School of Bioresources and Technology, King Mongkut's University of Technology Thonburi (Bang Khun Thian Campus), 49 Soi Thian Thale 25, Bang Khun Thian Chai Thale Rd., Tha Kham, Bang Khun Thian, Bangkok, Thailand, 10150, [4]Bioinformatics and Systems Biology program, King Mongkut's University of Technology Thonburi (Bang Khun Thian Campus), 49 Soi Thian Thale 25, Bang Khun Thian Chai Thale Rd., Tha Kham, Bang Khun Thian, Bangkok, Thailand, 10150.

Kalata B1 has been demonstrated to have bioactivity relating to membrane disruption. In this study, we conducted coarse-grained molecular dynamics simulations to gain further insight into kB1 bioactivity. The simulations were performed at various concentrations of kB1 to capture the overall progression of its activity. Two configurations of kB1 oligomers, termed tower-like and wall-like clusters, were detected. The conjugation between the wall-like oligomers resulted in the formation of a ring-like hollow in the kB1 cluster on the membrane surface. Our results indicated that the molecules of kB1 were trapped at the membrane-water interface. The interfacial membrane binding of kB1 induced a positive membrane curvature, and the lipids were eventually extracted from the membrane through the kB1 ring-like hollow into the space inside the kB1 cluster. These findings provide an alternative view of the mechanism of kB1 bioactivity that corresponds with the concept of an interfacial bioactivity model.

Cyclotides are 28–37 amino acids peptides found in various plants, such as Rubiaceae, Violaceae, Cucurbitaceae and Apocynaceae[1]. These peptides are classified into the Möbius, Bracelet and Trypsin inhibitor subfamilies[1]. All cyclotides contain a cyclic cystine knot (CCK) motif, a defining characteristic that is a combination of a head-to-tail cyclic backbone and a knot of three disulfide bonds that connect six conserved cysteine residues[2–4]. The amino acid sequences between each pair of the conserved cysteines are termed loop 1–6[2]. Cyclotides are stable in various physical and chemical conditions as a result of the CCK motif[5,6]. This is an attractive property of these peptides that can be used as a scaffold for designing therapeutic peptides, especially for improving the stability of linear peptides[7–11]. In addition, these peptides display cytotoxicity to microbes[12], along with HIV-infected[13–15], cancer[16] and tumor[17] cells. However, their use as therapeutic agents remains limited because of their high toxicity to normal cells[8]. Therefore, many efforts have been made to study the mechanism of their activity[18–26].

Cyclotides are amphiphatic peptides with a partitioning between the clusters of hydrophobic and hydrophilic amino acid residues on their surface[22]. These clusters are responsible for the membrane binding[19–21] and self-assembly[22] of the peptides, which are fundamental steps in their activity[18,22–24]. Furthermore, it has been proposed that cyclotides are able to penetrate the membrane, causing the formation of "barrel-stave" or "toroidal" membrane pores with an estimated diameter of 4.1–4.7 nm[23,26]. The activity of cyclotides is also involved with the depletion of membrane lipids[25], which is believed to be due to the solubilization of membrane lipids by the peptide[26]. Based on those findings, Wang and colleagues[26] have proposed a model to describe the overall mechanism of the activity of kalata B1 (kB1)–a cyclotide in the Möbius subfamily.

Recently, the molecular dynamics (MD) simulation method, which provides details of molecular motions and interactions as a function of time, has been widely used to study the dynamic interactions of biological macromolecules[27,28]. A modern MD simulation technique known as coarse-grained molecular dynamics (CG-MD) simulation has been successfully used to study heterogeneous membrane models[29], which is an updated model of

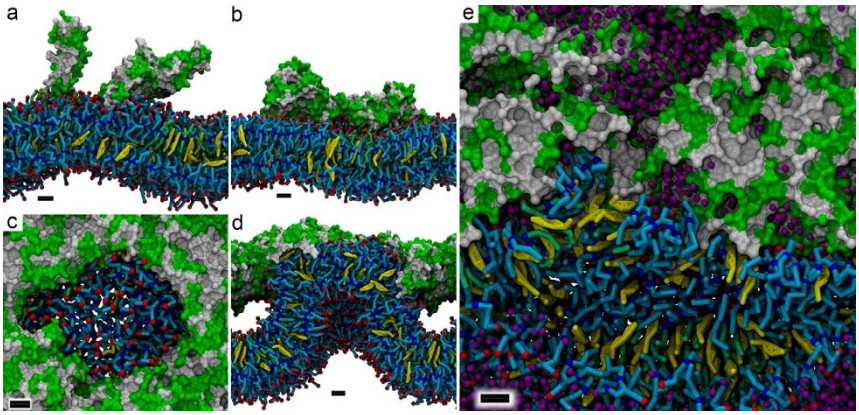

Figure 1 | Progressive membrane association and disruption activity of kB1. The binding of (a) the tower-like and (b) wall-like oligomer of kB1 to the membrane-water interface. (c) and (d) The top and side view of the ring-like hollow in the kB1 cluster at the membrane surface of 120 kB1 molecules indicating the curvature of the membrane induced by the binding of kB1, by which lipids covered by the ring-like hollow were at the same level as the kB1 cluster. (e) The side-view snapshot of the simulation of 350 kB1 molecules with the membrane indicates that lipids were extracted from the membrane via the ring-like hollow at the membrane surface and moved to the space inside the kB1 cluster. For all snapshots, the hydrophobic and hydrophilic residues of kB1 are represented by white and green colors, respectively. DPPC, DUPC and CHOL are colored as lime, cyan and yellow, respectively. Head (NC3) and first acyl-chain carbon (C1A and C1B) atoms of DPPC and DUPC are shown as red and blue color, respectively. Molecules of kB1 are shown as surface models. Lipid molecules are represented as licorice models. To clarify the picture, water molecules are not shown, except (e) that water molecules are shown with a violet color to indicate spaces inside the kB1 cluster. Each scale bar is equal to 1 nm.

biological cell membrane[30]. The organization of various peptides upon bonding with the membrane model has also been reported[31,32]. In addition, the aggregation behavior of cyclic antibacterial peptides, which leads to membrane disruption, has also been successfully described using CG-MD simulations[33]. Accordingly, we applied CG-MD simulations to dynamically investigate the mechanism of kB1 activity in relation to the membrane disruption. In this study, the simulations were performed at various concentrations of kB1 (Supplementary Table S1 online). A simulation of 24 molecules of kB1 (type 1 simulation) was initially performed to understand the progressive oligomerization of kB1. The membrane disruption activity of kB1 was further observed at higher concentrations of kB1. In addition, the effect of the aggregation behavior of kB1 on membrane disruption activity was investigated in this study. Therefore, the concentration of kB1 was increased in two different manners. First, the concentration of kB1 was increased stepwise from 24 to 48, 72, 96 and 120 molecules (type 2 simulation). Second, a set of simulations with 48, 72, 96 and 120 molecules of kB1 were separately performed (type 3 simulations). An additional simulation with 350 kB1 molecules was further performed to investigate the membrane lipid extraction activity of kB1. Consequently, an alternative view of the mechanism of kB1 activity that resembles the concept of the interfacial activity model[34], which is a non-pore membrane disruption model[35], was demonstrated (Fig. 1).

Results

Behavior of kB1 oligomers. An analytic ultracentrifugation study indicated the ability of cyclotides to form oligomers[18]. Another study demonstrated that the lateral diffusion of kB1 on the membrane surface allowed the peptide to form an oligomer containing 16–24 kB1 molecules that was able to form a ring in the membrane[23]. Here, the formation and behavior of kB1 oligomers during their association with the membrane were examined with a simulation of 24 kB1 molecules (type 1 simulation). Initially, dimers, tetramers and octamers were determined to be the majority of the oligomeric forms (Figs. 2a and b). Afterwards, oligomers containing 12, 16 and 24 kB1 molecules were continuously formed (Figs. 2c–e, respectively). Once the 24-mer was formed, the kB1 molecules did not disassociate (Supplementary Fig. S1 online). These results indicate that the number of kB1 molecules in an oligomer was an even number and a factor of the tetramer or octamer, which agrees with the results suggested in (ref. 23). In addition, the analysis indicated that the oligomers grew quickly during 0–0.14 μs, when most of the kB1 molecules or oligomers were in the water. After that time period (0.15–1.88 μs), the oligomers grew slowly when most of the kB1 molecules were bonded to the membrane.

For 60 μs during the type 1 simulation, we detected two main configurations of kB1 oligomers, termed tower-like and wall-like clusters (Figs. 1a and b, respectively). The tower-like oligomers were detected during the early period of the simulation, when the kB1 oligomers in the water bonded to other kB1 molecules or oligomers

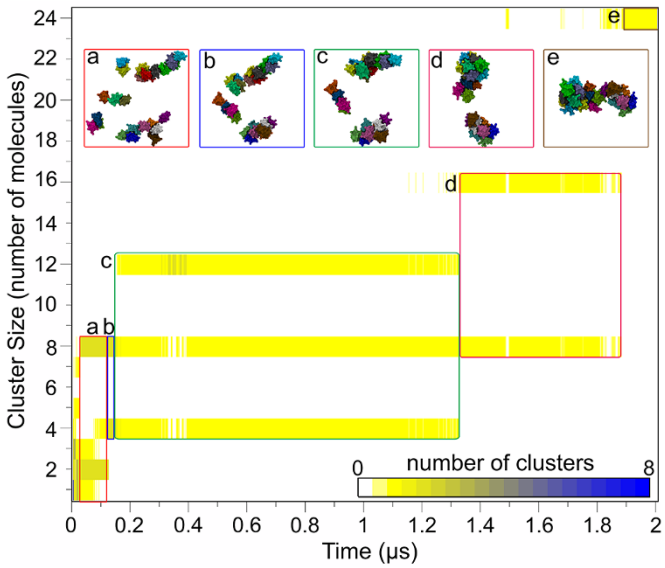

Figure 2 | Clustering behavior of kB1 molecules. The size of the kB1 clusters is plotted as a function of time during the first 2 μs of the type 1 simulation, whereas the number of the clusters in each cluster size is represented by the color (see color scale bar). The plot for the full time of the simulation is shown in Supplementary Fig. S1 online. Snapshots for each period of time are labeled and covered by the same letter and box color as those shown in the plot. Molecules of kB1 are shown as surface models and are colored by molecular chains.

at the membrane surface, resulting in vertically-grown oligomers. The tower-like oligomers were then transformed to the wall-like oligomers, where most of the kB1 molecules were bonded with the membrane and longitudinally arranged along the membrane surface. When the concentration of kB1 was increased (type 2 and 3 simulations), the wall-like clusters were elongated (Fig. 3). When 120 kB1 molecules were simulated, the conjugation between the wall-like clusters resulted in the formation of a ring-like hollow in the kB1 cluster ('ring-like' refers to a closed ring made by the connection of kB1 molecules and 'hollow' refers to space inside the kB1 ring, see Fig. 1c). The hollow was located on the membrane surface because kB1 interfacially bound to the membrane. The diameter of the ring-like hollow detected in the type 2 simulation was approximately 13 nm (Fig. 3e), whereas the diameter detected in the type 3 simulations was approximately 5.5 nm (Figs. 1c and 3i), which was closer to 4.1–4.7 nm estimated by Huang et al. (ref. 23).

Interfacial membrane binding of kB1. The distance between the COM of each peptide molecule to that of the membrane was measured to determine the position of the peptides relative to the membrane. We observed that there were no kB1 molecules in any simulation that penetrated the membrane (Fig. 4). The average distances from the center of mass (COM) of the membrane-bound kB1 molecules in the type 1 simulation, for example, to that of the membrane during 50–60 μs of the simulation were in the range of 2.2 ± 0.3(s.d.) and 4.3 ± 0.3(s.d.) nm (with minimum and maximum values of 1.4 and 5.2 nm from the raw data, respectively), in which the relative distance of the lipids head, glycerol and first acyl-chain carbon (C1A and C1B) atoms of the membrane were 1.9 ± 0.0(s.d.), 1.4 ± 0.0(s.d.) and 1.1 ± 0.0(s.d.) nm, respectively. These results demonstrate that kB1 molecules were located at the membrane-water interface.

Membrane deformation by kB1. To investigate the membrane disruption activity of kB1, membrane properties changing due to the binding of kB1s was observed. Instead of penetrating the membrane, the simulations indicated that kB1 induced membrane curvature. The membrane curvature degree was calculated by measuring the distance of every lipid head atom relative to the COM of the membrane. Thereby, the positions of all lipid head atoms relative to the COM of the membrane were determined (Fig. 4). The results indicated that the curvature could be detected even when the membrane was not bound with kB1 molecules (Fig. 4a). The frequency distribution analysis of the distance values revealed two main peaks of the distribution graph at 2.0 and −2.0 nm, reflecting the upper and lower surfaces of the kB1-free membrane, respectively (Supplementary Fig. S2 online). The maximum distances relative to the COM of the membrane of this system were 3.2 and −3.5 nm for the positive (up-curving) and negative (down-curving) curvature, respectively. These results indicate the predominantly negative curvature of the kB1-free membrane. However, when the membrane was bound with 24 molecules of kB1, the maximum distance for the positive and negative curvatures, which averaged over 60 μs in the type 1 simulation, increased by 16% (3.7 ± 0.4(s.d.) nm) and 3% (−3.6 ± 0.2(s.d.) nm), respectively. These results indicate that the membrane binding of kB1 dominantly induced positive curvature. Furthermore, the results from the type 1 (Fig. 4b), type 2 (Fig. 4c–f) and type 3 (Fig. 4g–j) simulations were compared to determine the relationship between the concentration of kB1 and the degree of the membrane curvature. The data in Table 1 indicate that the peak-to-peak amplitudes of the membrane curve with 48, 72, 96 and 120 kB1 molecules in the type 2 simulations increased by approximately 4, 16, 28 and 49% from that of the type 1 simulation during the same period of measured time (12 μs), respectively. In addition, the results also indicated that the membrane curvature of the type 2 simulation was increased both in the positive and negative direction and spanned on a large area of the membrane (Fig. 4 and Supplementary Fig. S2 online). However, the peak-to-peak amplitudes with 48, 72 and 96 kB1 molecules in the type 3 simulations (Fig. 4g–i) decreased by 17, 21 and 2% from that of the type 2 simulation at the same concentration, respectively. Correspondingly, the data in Table 1 indicate that the number of kB1 molecules that bound with the membrane in the type 3 simulations was lower than that observed in the type 2 simulation at the same concentration. The results demonstrated that the degree of the membrane curvature was directly affected by the number of kB1 that associate with the membrane. Surprisingly, the membrane curvature degree with 120 kB1 molecules in the type 3 simulation (Fig. 4J) was 85%

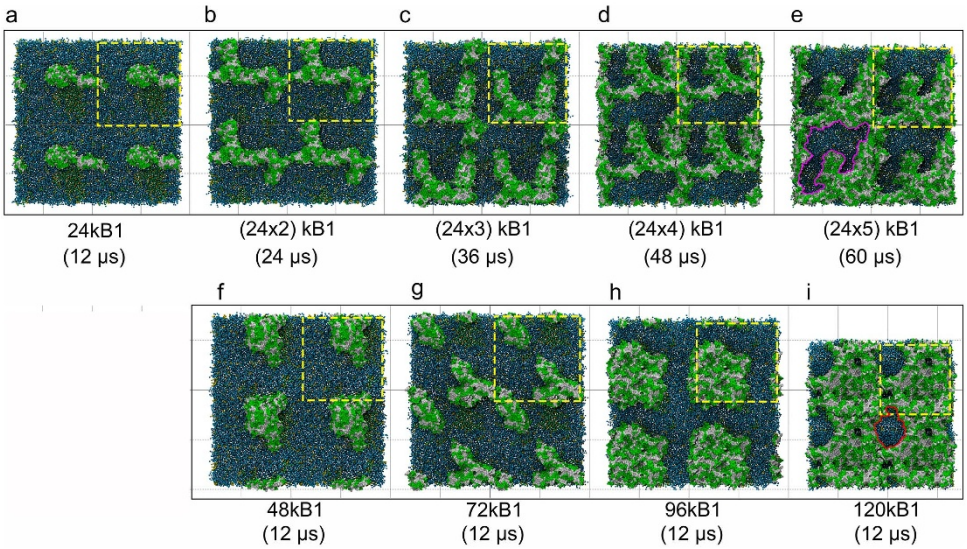

Figure 3 | Different oligomerization behaviors of kB1. (a) The top view snapshot at 12 μs of the type 1 simulation indicates short wall-like clusters on the membrane surface. (b–e) The wall-like clusters were continuously elongated when the concentration of kB1 was increased to 48, 72, 96 and 120 molecules in the type 2 simulation. (f–i) The large oligomers were detected on the membrane surface of the type 3 simulations. The representation is the same as in Fig. 1, except that the NC3, C1A and C1B atoms are not highlighted. The pink line shown in (e) represents a ring-like hollow in the kB1 cluster with a diameter of ~13 nm, whereas the red line in (i) shows a ring-like hollow in the kB1 cluster with a diameter of ~5.5 nm. Yellow dashed-line boxes represent central simulation cells in a four-periodical image of each simulation system.

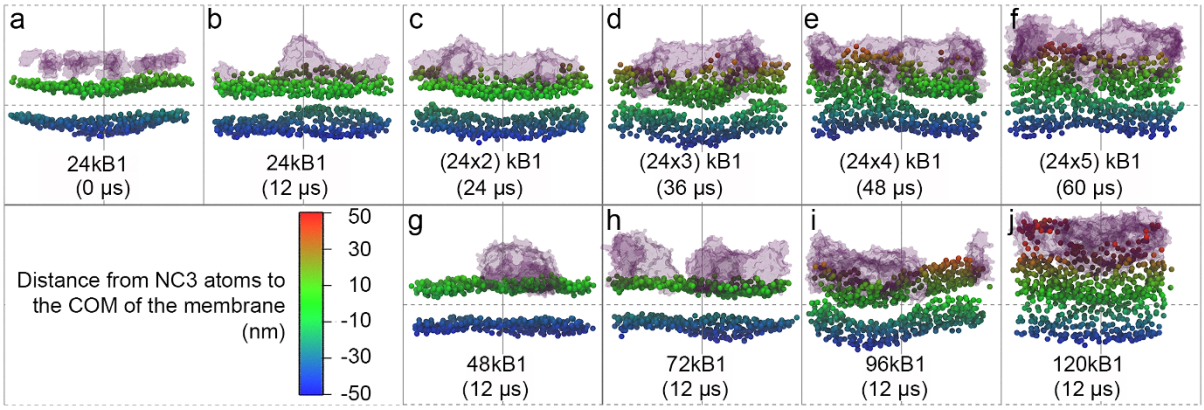

Figure 4 | Membrane curvature change due to the binding of kB1. The membrane curvatures at various kB1 concentrations and simulation times are represented by positions of all lipid head (NC3) atoms for both upper and lower leaflets of the membrane relative to the COM of the membrane. The color of each lipid head atom is represented by its distance relative to the COM of the membrane (see color scale bar). The kB1 molecules are shown as transparent surfaces with a violet color on the top of the membrane surface. Top view snapshots of (b–j) are shown in Figs. 3a–i.

higher than that of the type 1 simulation at 12 μs (Fig. 4b). In addition, the value was increased by 25% from that of the type 2 simulation at the same concentration (Fig. 4f), although the number of the membrane-bound kB1 molecules in the type 3 simulations was lower than that observed in the type 2 simulation (Table 1). The side-view snapshot of the ring-like hollow in the kB1 cluster in the type 3 simulations indicates a relationship between the ring-like hollow formation and the degree of the membrane curvature because it showed that the membrane in the area that surrounded by the ring-like hollow (which was the highest membrane curve among all systems) was at the same height level as the kB1 molecules that forming the ring-like hollow (Fig. 1d). Quantitatively, the relative position between the membrane and kB1 cluster was represented by their time series hydrophobicity ratio (Fig. 5), which was measured perpendicularly to the membrane surface (see Supplementary Fig. S3 online for details of the measurement). The hydrophobicity ratio can also represent thickness change of the membrane. Initially, the thickness of the membrane was ca. 5 nm (see Fig. 5a), where the lower and upper surface of the membrane were located at ca. 5 and 10 nm along the Z axis of the simulation box, respectively. The hydrophobicity ratio at the membrane core was in range of 0.8–1 while those of upper and lower hydrophilic layers were in range of 0.6–0.1. The membrane thickness was then rapidly increased to approximately 16 nm. This thickness change was a result of the membrane curvature, as indicated by the lower hydrophobicity ratio at the center of the thickness-increasing area of the membrane (see dashed-line box) compared with that at the core of the membrane at 0 μs. Interestingly, 85% of the total increase of the thickness occurred in the upper layer, whereas only 15% was detected in the lower layer of the membrane, indicating a dominant positive curvature over the negative curvature. For the cluster of kB1 molecules of the same system as the membrane (Fig. 5b), the hydrophobicity ratio was high at the bottom region of the cluster (see solid-line box). The kB1 molecules in this region bound with the membrane. However, a low hydrophobicity ratio was also detected at the lowest area of this region because some kB1 molecules in this area could not bind to the membrane due to the membrane curvature (Fig. 1d for snapshot). A low hydrophobicity ratio was also detected at the top of the kB1 cluster, which was the region that kB1 molecules interacted with the water. In contrast, the hydrophobicity ratio at the core of the kB1 cluster was in range of 0.5–0.6. In the beginning of the simulation (the curvature was not present in the membrane) the kB1 cluster was on top of the membrane and its hydrophobicity-plot area was slightly overlapped with that of the membrane (see Fig. 5a and b during 0–0.1 μs at ca. 8–9 nm of the Z axis). This corresponds with the interfacial membrane binding of kB1. Interestingly, when the membrane curvature was induced by kB1, the thickness-increasing area of the membrane (ca.

Table 1 | Summary of membrane curvature changes of the three simulation types related to kB1 concentration. 'Max' refers to the maximum points of the positive membrane curvature where 'Min' refers to the minimum points of the negative membrane curvature. 'Peak-to-Peak amplitude' is the distance between Max and Min points. Values of 'The number of membrane-bound kB1', 'Max' and 'Min' are a time-averaged values, and the error estimation is shown as standard deviation

Simulation type	Time (μs)	Total number of kB1 (molecule)	The number of membrane-bound kB1 (molecule)	Max (nm)	Min (nm)	Peak-to-Peak amplitude (nm)
Type 1	0–12	24	9 ± 1	3.6 ± 0.3	−3.7 ± 0.2	7.3
	12–24	24	8 ± 1	3.9 ± 0.4	−3.6 ± 0.2	7.5
	24–36	24	11 ± 1	4.0 ± 0.4	−3.7 ± 0.2	7.7
	36–48	24	8 ± 1	3.7 ± 0.3	−3.5 ± 0.2	7.2
	48–60	24	8 ± 1	3.4 ± 0.3	−3.4 ± 0.2	6.8
Type 2	12–24	(24 × 2)	21 ± 1	3.9 ± 0.3	−3.9 ± 0.2	7.8
	24–36	(24 × 3)	25 ± 3	4.8 ± 0.3	−4.1 ± 0.3	8.9
	36–48	(24 × 4)	28 ± 2	4.9 ± 0.2	−4.3 ± 0.2	9.2
	48–60	(24 × 5)	32 ± 2	5.2 ± 0.3	−4.9 ± 0.2	10.1
Type 3	0–12	48	10 ± 1	3.2 ± 0.2	−3.3 ± 0.2	6.5
	0–12	72	16 ± 1	3.4 ± 0.2	−3.6 ± 0.2	7
	0–12	96	19 ± 2	4.6 ± 0.2	−4.4 ± 0.2	9
	0–12	120	23 ± 2	6.8 ± 0.2	−5.8 ± 0.2	12.6

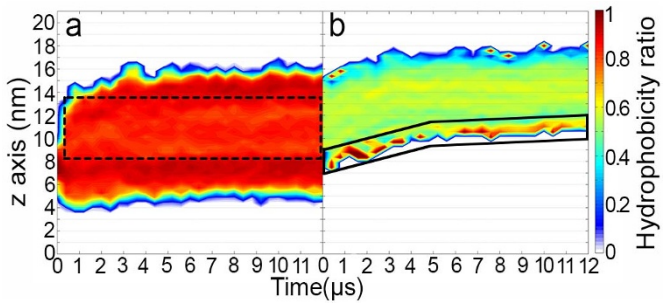

Figure 5 | The membrane was lifted to the kB1 cluster. The hydrophobicity ratio of (a) the membrane and (b) a cluster of 120 kB1 molecules located on the membrane surface were measured along the Z axis of the system (see Supplementary Fig. S3 online). A dashed-line box covers the hydrophobicity ratio at the thickness-increasing area of the membrane. A solid-line box covers hydrophobicity ratio at the bottom region of the kB1 cluster. The Y axis of the heat map represents overall thickness (Z axis) of the simulation box.

10–16 nm in the Z axis) significantly overlapped with the area of the kB1 cluster, whereas the position of the kB1 cluster was slightly higher during 0–3 μs. These results clearly indicate that kB1 molecules did not deeply penetrate the membrane. Instead, the membrane was curved up onto the kB1 cluster.

Membrane lipid extraction by kB1. An additional simulation was further performed with 350 molecules of kB1 according to the kB1 molecule per lipid ratio of 0.35 that caused 50% lipid vesicle leakage, as calculated from the graph showing the relationship between the ratio of kB1 with membrane lipids and bioactivity of the peptide[23]. Membrane behavior similar to that previously described was also detected in this system. Additionally, the membrane lipid extraction was further analyzed by comparing the position of lipid residue 296 (as an example) with the COM of the membrane and that of the membrane surface. Positions of sample lipid, the whole membrane, and the membrane surface were obtained by measured distance from their COM to the reference point (see Supplementary Fig. S4a online). The results showed that the distances from the COM of the whole membrane and that of the membrane surface to the reference point were continuously increased as a result of the positive curvature. Simultaneously, the distance of lipid residue 296 relative to the reference point was also increased (Fig. 6a and b). The distance increase of the COM of lipid residue 296 was steady during 1–12 μs. Therefore, to observe the increasing rate of the distance, the distance values of lipid residue 296, the whole membrane, and the membrane surface were fitted using a linear equation during this time period. The results indicated that the slope of the linear fitting curve for lipid residue 296 (0.27) was approximately 2 and 3-fold higher than that of the whole membrane (0.14) and that of the membrane surface (0.10), respectively (Fig. 6a). Similar results were also observed in other sample lipids (Fig. 6b and Supplementary Fig. S4b online), implying that lipid residue 296 and other lipids were extracted from the membrane.

Discussion

Although the mechanism of kB1 activity has been extensively studied and several models have been proposed to depict the overview of the mechanism, the intensive dynamic and molecular details of the mechanism that could provide a deeper insight have not yet been reported. Here, CG-MD simulations were conducted to demonstrate progressive membrane association, oligomerization and membrane disruption activity of kB1. Based on the results from the MD simulations, we propose an alternative view of the mechanism of kB1 activity. Fig. 1 shows the overall membrane disruption progression of the newly proposed model. The membrane disruption activity of kB1 molecules is initiated by their binding to the membrane. We observed that some kB1 molecules directly bound to the membrane, and some other molecules formed oligomers in the water. In addition, the results suggest that the tetramer was a building block of the oligomer. The kB1 oligomers in the water then bound to the membrane surface, forming tower-like clusters (Fig. 1a). During this period (0–0.14 μs), the oligomers quickly grew compared with the later period (0.15–1.88 μs) when most of kB1 molecules bound to the membrane. This result was likely because kB1 in the water could move and rotate in all directions to interact with other kB1 molecules. In contrast, the membrane-bound kB1 molecules could only move on the plane of the membrane surface, thus reducing their probability of interacting with others. However, the hydrophobic residues of kB1 molecules that formed the towers were mostly exposed to the water (Fig. 1a). The tower-like clusters were then transformed to the wall-like cluster to bury the hydrophobic residues in the membrane (Fig. 1b). When the concentration of kB1 was increased, the wall-like cluster was then elongated by connecting with other wall clusters and eventually forming the ring-like hollow in the kB1 cluster on the membrane surface (Fig. 3). However, we observed that a different manner of kB1 concentration increasing could affect the ring-like hollow formation. In the type 2 simulation, the kB1 molecules that were stepwise increased formed small oligomer(s) in the water before binding to the membrane and then laterally moved to interact with other oligomers (Figs. 3a–e). This allowed for the scattering of kB1 molecules on the membrane surface and resulted in the formation of the large ring-like hollow in the kB1 cluster (Fig. 3e). In contrast, kB1 molecules in the type 3 simulations reached the membrane as large oligomers. Therefore, the smaller ring could be formed more easily in this simulation type because the kB1 molecules were less scattered in this system, and thus, a long-distance lateral movement of kB1 was not required (Figs. 3f–i).

Wang and colleagues proposed that kB1 molecules are able to permeate the membrane to form pores in the membrane[26]. Nevertheless, the dynamics and molecular details of the kB1-membrane interaction obtained in this study demonstrated that kB1 molecules did not penetrate the membrane and were trapped at the membrane surface. We observed that kB1 molecules were located at the membrane interfacial zone, which is the region at the membrane-water interface and has a thickness of 1.0–1.5 nm covering the water area, where the membrane is polar, with small portions of hydrophobic atoms[34]. Therefore, the insertion of kB1 in this zone could be described by the partitioning of hydrophobic and hydrophilic patches on the peptide surface. We performed a short simulation of one kB1 molecule with the membrane to verify this assumption and found that with the membrane-bound state, approximately 55.84% and 44.16% of the total interaction energy of the kB1 monomer accounted for the kB1-membrane and kB1-water interaction energy, respectively (Supplementary Fig. S5 online). These results indicate that although the hydrophobic patch was inserted into the membrane, nearly half of its structure, which was the hydrophilic patch, preferentially interacted with the water. In addition, our study used the same simulation force field (MARTINI CG force field[36–38]) as that used in (ref. 39), which demonstrated that two of the three forms of cardiotoxin A3, the Cobra Cytotoxin, which has a configuration similar to that of cyclotides, lack membrane penetration ability while another form is able to permeate the membrane[39]. Therefore, the lacking of membrane penetration ability of kB1 should not be a result of the use of MARTINI CG force field.

Instead of penetrating the membrane, kB1 molecules began disrupting the membrane by inducing curvature in the membrane while they were still on the membrane surface. In fact, the membrane curvature could be detected even when the membrane was not bound with kB1 molecules (Fig. 4a). Negative curvature was observed at the CHOL-enriched domain of the kB1-free membrane, which is consistent with the fact that the existence of small lipids, such as choles-

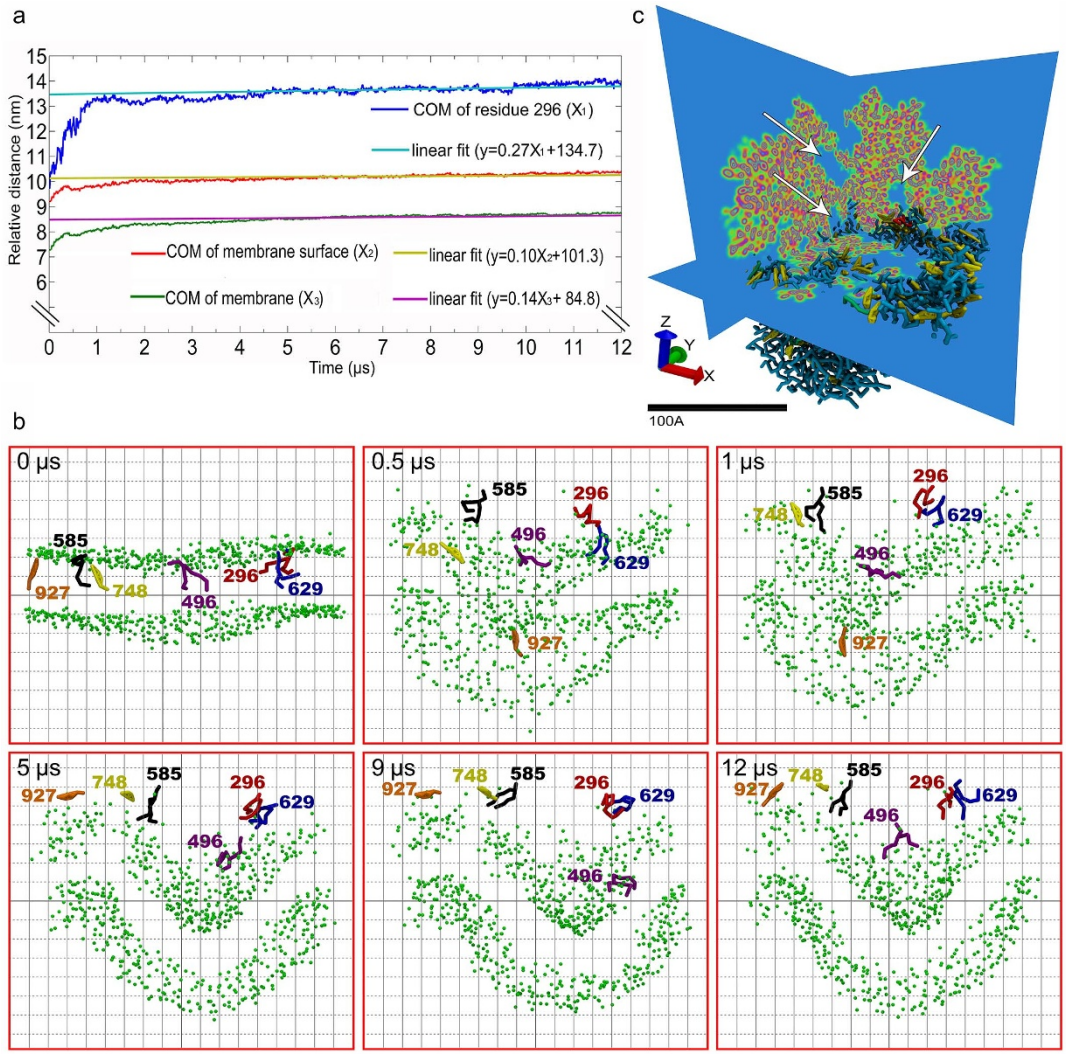

Figure 6 | Membrane lipid extraction by kB1. (a) The distance of the COM of a sample lipid (lipid residue 296) and the COM of the whole membrane, as well as that of the membrane surface to the reference point, are plotted as a function of time. Green, red and blue lines show the distance from the COM of the whole membrane, the membrane surface and lipid residue 296 to the reference point, respectively. Pink, yellow and cyan lines show the linear fitted curve of the distance values of the whole membrane, the membrane surface and lipid residue 296, respectively. (b) NC3 atoms of DPPC and DUPC in upper and lower layers of membrane are shown as green balls. Lipid residue 296, 496, 585, 629, 748 and 927 are shown as a CPK model with red, violet, black, blue, yellow and orange colors, respectively. Size of each grid space is 1 × 1 nm. (c) The volume matrix slides in the X, Y and Z planes of the system show the cross-section surface inside the kB1 cluster. The areas occupied by kB1 molecules are shown as small dots on the volumetric slides, whereas the spaces inside kB1 cluster are indicated by the arrows. Lipid residue 296 is shown as a licorice model with a red color. Other lipids in the membrane are also shown as licorice models with the same color as shown in Fig. 3.

terol, at some local areas on the membrane could result in negative membrane curvature at that area[40]. In contrast, when the membrane was bound with kB1, positive curvature was detected in the majority areas. The curvature degree (height of the curve) was directly dependent on the number of kB1 molecules that interfacially bound with the membrane (Table 1). These results are consistent with reports (ref. 40, 41) that demonstrated that the asymmetric membrane binding of amphipathic peptides with high local density can result in membrane curvature. Furthermore, the insertion of peptides into approximately 16% of the total thickness of the membrane hydrophobic region resulted in a positive curvature, whereas a negative curvature occurred when the insertion depth was 42% of the thickness[42]. We then measured the distance of the COM of kB1 to that of the membrane to explore insertion dept of kB1 in membrane and observed the distance of 2.2 ± 0.3(s.d.) which was the area occupied by the lipid head atoms (Supplementary Fig. S6 online). We also calculated the distance of Trp19, which is the largest residue of kB1 that inserted into the membrane, to the COM of the membrane in order to measure the deepest distance that a kB1 molecule can insert into membrane. The results indicate that the average insertion depth of Trp19 of single kB1 molecule was 1.7 ± 0.4(s.d.) nm relative to the COM of the membrane (Supplementary Fig. S6 online). Thus, Trp19 was inserted into approximately 7% of the hydrophobic region, as calculated from the lower bound of the average value of 1.3 nm when GL atoms were considered as the surface of the membrane hydrophobic region. These results indicate that the partial insertion of kB1 into the membrane interfacial zone was responsible for the membrane curvature, especially the positive curvature.

However, the membrane curvature was more dominantly related to the formation of the ring-like hollow in the kB1 cluster of kB1 at the membrane surface. In the type 3 simulations at 120 molecules of kB1, we observed a ring-like hollow with a diameter nearly identical to that reported with the experiment[23] (Fig. 1c and 3i). We also observed that the membrane in the area that surrounded by the ring-like hollow (which was the highest curvature area among all

simulation systems) was curved to the same level as the kB1 that formed the ring-like hollow (Fig. 1d). This relative position between kB1 molecules and the membrane, i.e., position of kB1 molecules were lower than the upper surface of the membrane (see results and Fig. 5), is similar to the results reported in (ref. 26). However, the movement of the membrane was limited in (ref. 26) because it was held on the support surface according to the neutron reflectometry method used in that study, and it was proposed that the cyclotides completely inserted and penetrated into the membrane[26]. In contrast, both the kB1 and membrane in our study were freely dynamic, and we molecularly demonstrated that kB1 did not penetrate the membrane; it was the membrane that curved up onto the kB1 cluster.

Burman and colleagues demonstrated that cyO2 in the Bracelet subfamily of cyclotides was able to extract lipids from the membrane[25]. Our results consistently demonstrated that kB1, even if it is a member of different subfamily, also displayed membrane lipid extraction activity. Our results indicated that kB1 molecules formed a large cluster on the membrane surface. Moreover, an analysis of kB1 occupancy demonstrated that there were spherical spaces occupied by water molecules inside the kB1 cluster and were connected to the ring-like hollows at the membrane surface (Fig. 6c). The overlaying of the volumetric slide of the kB1 occupancy to the membrane surface indicated that the lipids were extracted from the membrane through the kB1 ring-like hollow at the membrane surface and then moved into spaces inside the kB1 cluster (Fig. 6b and c). Therefore, it can be said that the ring-like hollow in the kB1 cluster was a starting area of membrane disruption by kB1. The movement of lipids from the membrane to the kB1 cluster was possibly involved with hydrophobicity distribution in the kB1 cluster. The ratios between hydrophobic and hydrophilic atoms at the core of the kB1 cluster were 0.53 $\pm$ 0.03(s.d.) and 0.47 $\pm$ 0.03(s.d.), respectively (Fig. 5b). This might have resulted in stepwise movement of lipids in the kB1 cluster by which acyl-chains of the lipids were attracted by hydrophobic residues while lipid head groups were attracted by hydrophilic residues. However, the hydrophobic mismatch between the lipids and kB1 molecules in the cluster could have occurred because the hydrophobicity ratio in the oligomers was not substantially different. Thus, there could have been continuous movement of lipids due to the chain of favorable and unfavorable hydrophobic interactions (Fig. 6b).

In summary, the mechanism obtained in this study reflects an interfacial activity model that used to describe the activity of antimicrobial peptides[34,35]. The interfacial activity model describes the ability of a molecule to bind to the membrane, partition into the membrane-water interface, and alter the packing and organization of the lipids[34]. In addition, this model was characterized as a non-pore model for the membrane disruption activity of antimicrobial peptides[35]. Thus, our study provides an alternative view of the mechanism of kB1 activity.

Methods

All of the simulations were conducted with the GROMACS software package[43,44] using the MARTINI CG force field[36–38]. The CG model is a molecular representation technique that reduces the number of atoms in the system by mapping a set of atoms into pseudo-atoms[37] and is thus suitable for long simulations and complex processes of peptide-membrane interactions[45]. The simulation integration was performed using a leap frog algorithm with a time step of 20 femtoseconds. The temperature was independently coupled for each molecule in the system to 310 K using the Berendsen thermostat[46]. The pressure was coupled to 1 atm using the semi-isotropic scheme of the Berendsen barostat[46], where the x, y plane and the z direction were coupled separately to obtain a tensionless membrane. The periodic boundary condition with standard non-bonded interaction criteria was applied to all systems. Visual Molecular Dynamics (VMD) software version 1.8.6[47] was used for system visualization and analysis. Because the simulations were performed based on a CG model, the time shown in the results was scaled by a factor of 4 (see ref. 29 for details).

Preparation of the KB1 CG model. Atomic coordinates of KB1 were obtained from the Protein Data Bank (PDB code 1NB1)[3]. The file "atom1Cg_v2.1.awk" was downloaded from the MARTINI website and used to convert the atomic coordinates to a CG coordinate file. Most of the amino acid residues were represented by two pseudo-atoms, one for the main chain and one for the side chain. Tryptophan was represented by five pseudo-atoms, one for the main chain and four for the aromatic side chain. Arginine was represented by three pseudo-atoms, one for the main chain and two for the longer side chain, whereas glycine was represented by one pseudo-atom showing only the main chain. The amino acid sequence and the secondary structure information were used as the input of "seq2itp.pl" to generate the GROMACS topology file. The sequence was obtained from the Protein Data Bank, and the secondary structure information was prepared using the GROMACS utility program do_dssp. Two additional options of "cysteines" and "elasticin" from the seq2itp.pl script were used to automatically define the disulfide bond and local elastic networks for kB1. Because the N and C termini of kB1 are closed by a peptide bond, the generated topology file was further modified to reflect this. Based on the sequence of 1NB1, in which the N terminus is cysteine and the C terminus is valine, all bond parameters of Val21 connecting with Cys 22 were used to describe the peptide bond of Val29 with Cys1. In this work, all simulations were performed at a pH equal to 7, and thus, the net charge of kB1 was 0.

Preparation of the membrane model. The heterogeneous membrane model was constructed based on lipids ratio obtained from experimental study[48] in order to mimic the real cell membrane. The number of lipids model was calculated based on the percent of lipid composition of uninfected H9 cell membrane. For 100% of total phospholipids, approximately 9.8% were sphingolipids, and 90.2% were other phospholipids[48]. The cholesterol composition was expressed as the cholesterol-to-phospholipid (c/p) ratio of 0.476. Using CG-MARTINI force field[36–38], we applied the lipid composition regarding (ref. 29), including diundecanoyl-phosphatidylcholine (DUPC), dipalmitoyl-phosphatidylcholine (DPPC), represent saturated (sphingolipid) and unsaturated lipids, respectively, and cholesterol (CHOL). In our system, there are 1,000 lipid molecules with the DPPC : DUPC : CHOL ratio of 0.07 : 0.62 : 0.31. in total. The lipid system was hydrated by six water beads (equal to 24 real water molecules) per lipid molecule[49]. Structures and GROMACS topology files of these three lipids were obtained from the martini website (http://md.chem.rug.nl/cgmartini/). We started construct the membrane model by uploading single molecule of DUPC, DPPC and CHOL to the web service of our in-house software, Automated Membrane Generator (https://10.4.52.26/amg/). The program automatically generated lipid bilayer of DPPC and CHOL with the ratio of 1 : 1 based on the theoretical shape complementary described in (ref. 50). The domain was then surrounded by DUPC and the remaining CHOL. The output heterogeneous lipid bilayer was downloaded from the web service. The lipids ratio in the bilayer was modified to obtain the desired membrane. After energy minimization, a simulation of 100 ns was performed for system equilibration at a temperature of 310 K and pressure of 1 atm. The production run of the 4 μs simulations was conducted under the same conditions. The average DPPC : DUPC : CHOL ratio in the domain area of the constructed membrane model was about 0.53 $\pm$ 0.20(s.d.) : 0.07 $\pm$ 0.17(s.d.) : 0.39 $\pm$ 0.23(s.d.), which is nearly identical to that reported in (ref. 29). The thickness difference between the domain and non-domain area of the membrane was in the range of 0.4–0.7 nanometers, which was corresponded to that of previously observed in (refs. 29,51,52). To validate our membrane model, we increased the temperature up to 400 K to disorganize the lipid domain formation according (ref. 29). The temperature was then cooled down to 310 K. After energy minimization and equilibration, the production run of this system was performed for 20 μs. At this time the domain was reformed (Supplementary Fig. S7 online).

Simulations to investigate oligomerization and membrane disruption activity of kB1. Three simulation types relating to kB1 concentration were performed to investigate the progressive membrane binding, oligomerization and membrane disruption activity of kB1. Because the charge distribution on the surface of kB1 is asymmetrical, the molecules of the peptides were added into the system with random geometry orientation. The molecules of kB1 were randomly added into the system using the Genbox program (see http://manual.gromacs.org/current/online/genbox.html) close to the upper surface of the membrane. All simulation types were started with the same membrane, the membrane at 4 μs, which contained 1,000 lipids molecules and ca. 24,000 water molecules (equal to 96,000 real water molecules). For the type 2 simulation, the kB1 molecules were continuously added into the system every 12 μs by replacing water molecules. Then, the water molecules were added for each kB1 concentration to meet the desired amount of water molecules. Therefore, thickness and size of the systems increased when the number of kB1 molecules was increased (see Supplementary Table S1 online). In addition, we placed the membrane at about 10–20% lower than center of the simulation box in the Z axis and then placed the peptides on the top of the membrane.

Size analysis of the kB1 oligomer. The clustering of kB1 in the oligomer was analyzed using the GROMACS utility tool–g_clustsize (http://manual.gromacs.org/online/g_clustsize.html). The "-mol" option of the program was used for calculating the clustering of the molecules. The cut-off for the clustering (see "-cut" option) was 2.0, which we determined was the average distance between two kB1 molecules when bound together. The default settings for all other options of the program were used.

Analysis of hydrophobicity ratio. The system was divided into small slabs along the Z axis. The numbers of hydrophobic and hydrophilic atoms in each slab were counted for the membrane and kB1 clusters. The hydrophobic ratio was calculated by dividing the number of hydrophobic atoms by the total number atoms in each slab. The hydrophobic ratios in all slabs were combined together based on their position along

the Z axis. The process was repeated for every time step of the simulation (200 ps) and performed separately for kB1 and the membrane. This analysis was performed using a custom tcl-script implemented by using the VMD[47] library.

Analysis of the occupancy volume of kB1. The occupancy volume was calculated using the VolMap Plugin of the VMD[47] software (http://www.ks.uiuc.edu/Research/vmd/plugins/volmapgui/). The analysis was performed for all residues of all kB1 molecules. The volumetric data of the "map types" option was set to "density", with weighting on the occupancy. The values were set to 0.5 and 1.5 Å for the "resolution" and "atom size" options, respectively. The occupancy volume was averaged for all frames of the simulation. The volume was visualized using VMD "VolumeSlice" drawing method in the X, Y and Z axes of the system.

Analysis of the exposure of kB1 residues to water. The exposure of the kB1 residues was represented by the solvent accessible surface area (SASA), which was calculated for the hydrophobic, hydrophilic and all other residues of kB1. The SASAs were analyzed using the "g_sas" program of GROMACS. The solvent probe radius was set to 0.56 nm following the method used in (ref. 53).

1. Daly, N. L., Rosengren, K. J. & Craik, D. J. Discovery, structure and biological activities of cyclotides. *Adv Drug Deliv Rev* **61**, 918–930 (2009).
2. Craik, D. J., Daly, N. L., Bond, T. & Waine, C. Plant cyclotides: A unique family of cyclic and knotted proteins that defines the cyclic cystine knot structural motif. *J Mol Biol* **294**, 1327–1336 (1999).
3. Rosengren, K. J., Daly, N. L., Plan, M. R., Waine, C. & Craik, D. J. Twists, knots, and rings in proteins. Structural definition of the cyclotide framework. *J Biol Chem* **278**, 8606–8616 (2003).
4. Pelegrini, P. B., Quirino, B. F. & Franco, O. L. Plant cyclotides: an unusual class of defense compounds. *Peptides* **28**, 1475–1481 (2007).
5. Colgrave, M. L. & Craik, D. J. Thermal, chemical, and enzymatic stability of the cyclotide kalata B1: the importance of the cyclic cystine knot. *Biochemistry* **43**, 5965–5975 (2004).
6. Čemažar, M. & Craik, D. Factors Influencing the Stability of Cyclotides: Proteins with a Circular Backbone and Cystine Knot Motif. *Int J Pept Res Ther* **12**, 253–260 (2006).
7. Craik, D. J., Simonsen, S. & Daly, N. L. The cyclotides: novel macrocyclic peptides as scaffolds in drug design. *Curr Opin Drug Discov Devel* **5**, 251–260 (2002).
8. Daly, N. L. & Craik, D. J. Design and therapeutic applications of cyclotides. *Future Med Chem* **1**, 1613–1622 (2009).
9. Garcia, A. E. & Camarero, J. A. Biological activities of natural and engineered cyclotides, a novel molecular scaffold for peptide-based therapeutics. *Curr Mol Pharmacol* **3**, 153–163 (2010).
10. Jagadish, K. & Camarero, J. A. Cyclotides, a promising molecular scaffold for peptide-based therapeutics. *Biopolymers* **94**, 611–616 (2010).
11. Henriques, S. T. & Craik, D. J. Cyclotides as templates in drug design. *Drug Discov Today* **15**, 57–64 (2010).
12. Tam, J. P., Lu, Y. A., Yang, J. L. & Chiu, K. W. An unusual structural motif of antimicrobial peptides containing end-to-end macrocycle and cystine-knot disulfides. *Proc Natl Acad Sci U S A* **96**, 8913–8918 (1999).
13. Daly, N. L., Gustafson, K. R. & Craik, D. J. The role of the cyclic peptide backbone in the anti-HIV activity of the cyclotide kalata B1. *FEBS Lett* **574**, 69–72 (2004).
14. Wang, C. K. *et al.* Anti-HIV cyclotides from the Chinese medicinal herb Viola yedoensis. *J Nat Prod* **71**, 47–52 (2008).
15. Henriques, S. T. *et al.* Decoding the membrane activity of the cyclotide kalata B1: the importance of phosphatidylethanolamine phospholipids and lipid organization on hemolytic and anti-HIV activities. *J Biol Chem* **286**, 24231–24241 (2011).
16. Gerlach, S. L. *et al.* Anticancer and chemosensitizing abilities of cycloviolacin 02 from Viola odorata and psyle cyclotides from Psychotria leptothyrsa. *Biopolymers* **94**, 617–625 (2010).
17. Lindholm, P. *et al.* Cyclotides: a novel type of cytotoxic agents. *Mol Cancer Ther* **1**, 365–369 (2002).
18. Nourse, A., Trabi, M., Daly, N. L. & Craik, D. J. A comparison of the self-association behavior of the plant cyclotides kalata B1 and kalata B2 via analytical ultracentrifugation. *J Biol Chem* **279**, 562–570 (2004).
19. Kamimori, H., Hall, K., Craik, D. J. & Aguilar, M. I. Studies on the membrane interactions of the cyclotides kalata B1 and kalata B6 on model membrane systems by surface plasmon resonance. *Anal Biochem* **337**, 149–153 (2005).
20. Shenkarev, Z. O. *et al.* Conformation and mode of membrane interaction in cyclotides. Spatial structure of kalata B1 bound to a dodecylphosphocholine micelle. *FEBS J* **273**, 2658–2672 (2006).
21. Svangard, E. *et al.* Mechanism of action of cytotoxic cyclotides: cycloviolacin O2 disrupts lipid membranes. *J Nat Prod* **70**, 643–647 (2007).
22. Simonsen, S. M. *et al.* Alanine scanning mutagenesis of the prototypic cyclotide reveals a cluster of residues essential for bioactivity. *J Biol Chem* **283**, 9805–9813 (2008).
23. Huang, Y. H. *et al.* The Biological Activity of the Prototypic Cyclotide Kalata B1 Is Modulated by the Formation of Multimeric Pores. *J Biol Chem* **284**, 20699–20707 (2009).
24. Huang, Y. H., Colgrave, M. L., Clark, R. J., Kotze, A. C. & Craik, D. J. Lysine-scanning Mutagenesis Reveals an Amendable Face of the Cyclotide Kalata B1 for the Optimization of Nematocidal Activity. *J Biol Chem* **285**, 10797–10805 (2010).
25. Burman, R., Stromstedt, A. A., Malmsten, M. & Goransson, U. Cyclotide-membrane interactions: defining factors of membrane binding, depletion and disruption. *Biochim Biophys Acta* **1808**, 2665–2673 (2011).
26. Wang, C. K., Wacklin, H. P. & Craik, D. J. Cyclotides insert into lipid bilayers to form membrane pores and destabilize the membrane through hydrophobic and phosphoethanolamine-specific interactions. *J Biol Chem* **287**, 43884–43898 (2012).
27. Karplus, M. & McCammon, J. A. Molecular dynamics simulations of biomolecules. *Nat Struct Biol* **9**, 646–652 (2002).
28. Kandt, C., Ash, W. L. & Tieleman, D. P. Setting up and running molecular dynamics simulations of membrane proteins. *Methods* **41**, 475–488 (2007).
29. Risselada, H. J. & Marrink, S. J. The molecular face of lipid rafts in model membranes. *Proc Natl Acad Sci U S A* **105**, 17367–17372 (2008).
30. Pike, L. J. Rafts defined: a report on the Keystone Symposium on Lipid Rafts and Cell Function. *J Lipid Res* **47**, 1597–1598 (2006).
31. Schafer, L. V. *et al.* Lipid packing drives the segregation of transmembrane helices into disordered lipid domains in model membranes. *Proc Natl Acad Sci U S A* **108**, 1343–1348 (2011).
32. Janosi, L., Li, Z., Hancock, J. F. & Gorfe, A. A. Organization, dynamics, and segregation of Ras nanoclusters in membrane domains. *Proc Natl Acad Sci U S A* **109**, 8097–8102 (2012).
33. Khalfa, A. & Tarek, M. On the antibacterial action of cyclic peptides: insights from coarse-grained MD simulations. *J Phys Chem B* **114**, 2676–2684 (2010).
34. Wimley, W. C. Describing the mechanism of antimicrobial peptide action with the interfacial activity model. *ACS Chem Biol* **5**, 905–917 (2010).
35. Wimley, W. C. & Hristova, K. Antimicrobial peptides: successes, challenges and unanswered questions. *J Membr Biol* **239**, 27–34 (2011).
36. Marrink, S. J., de Vries, A. H. & Mark, A. E. Coarse Grained Model for Semiquantitative Lipid Simulations. *J. Phys. Chem. B* **108**, 750–760 (2003).
37. Marrink, S. J., Risselada, H. J., Yefimov, S., Tieleman, D. P. & de Vries, A. H. The MARTINI force field: coarse grained model for biomolecular simulations. *J Phys Chem B* **111**, 7812–7824 (2007).
38. Monticelli, L. *et al.* The MARTINI Coarse-Grained Force Field: Extension to Proteins. *J. Chem. Theory and Comput.* **4**, 819–834 (2008).
39. Su, Z. Y. & Wang, Y. T. Coarse-grained molecular dynamics simulations of cobra cytotoxin A3 interactions with a lipid bilayer: penetration of loops into membranes. *J Phys Chem B* **115**, 796–802 (2011).
40. Kirchhausen, T. Bending membranes. *Nat Cell Biol* **14**, 906–908 (2012).
41. Farsad, K. & De Camilli, P. Mechanisms of membrane deformation. *Curr Opin Cell Biol* **15**, 372–381 (2003).
42. Zemel, A., Ben-Shaul, A. & May, S. Modulation of the spontaneous curvature and bending rigidity of lipid membranes by interfacially adsorbed amphipathic peptides. *J Phys Chem B* **112**, 6988–6996 (2008).
43. Van Der Spoel, D. *et al.* GROMACS: fast, flexible, and free. *J Comput Chem* **26**, 1701–1718 (2005).
44. Hess, B., Kutzner, C., van der Spoel, D. & Lindahl, E. GROMACS 4: Algorithms for Highly Efficient, Load-Balanced, and Scalable Molecular Simulation. *J. Chem. Theory Comput.* **4**, 435–447 (2008).
45. Chng, C. P. & Yang, L. W. Coarse-grained models reveal functional dynamics--II. Molecular dynamics simulation at the coarse-grained level--theories and biological applications. *Bioinform Biol Insights* **2**, 171–185 (2008).
46. Berendsen, H. J. C. a. P., J. P. M., van Gunsteren, W. F., DiNola, A. & Haak, J. R. Molecular dynamics with coupling to an external bath. *J. Chem. Phys.* **81**, 3684–3690 (1984).
47. Humphrey, W., Dalke, A. & Schulten, K. VMD: visual molecular dynamics. *J Mol Graph* **14**, 27–38 (1996).
48. Aloia, R. C., Tian, H. & Jensen, F. C. Lipid composition and fluidity of the human immunodeficiency virus envelope and host cell plasma membranes. *Proc Natl Acad Sci U S A* **90**, 5181–5185 (1993).
49. Scott, K. A. *et al.* Coarse-Grained MD Simulations of Membrane Protein-Bilayer Self-Assembly. *Structure* **16**, 621–630 (2008).
50. Fantini, J., Garmy, N., Mahfoud, R. & Yahi, N. Lipid rafts: structure, function and role in HIV, Alzheimer's and prion diseases. *Expert Rev Mol Med* **4**, 1–22 (2002).
51. Niemela, P. S., Ollila, S., Hyvonen, M. T., Karttunen, M. & Vattulainen, I. Assessing the nature of lipid raft membranes. *PLoS Comput Biol* **3**, e34 (2007).
52. Rinia, H. A., Snel, M. M., van der Eerden, J. P. & de Kruijff, B. Visualizing detergent resistant domains in model membranes with atomic force microscopy. *FEBS Lett* **501**, 92–96 (2001).
53. Vuorela, T. *et al.* Role of lipids in spheroidal high density lipoproteins. *PLoS Comput Biol* **6**, e1000964 (2010).

Acknowledgments

The authors thank Kriengkrai Porkaew and Nitnipa Soontorngun for their insightful discussions and suggestions. We also thank Rungtiva Palangsuntikul and Thanyada Rungrotmongkol for their suggestions about the molecular dynamics simulations. We thank Julie Koldewyn and Brennan Barfuss for help in editing and proofreading the manuscript. We thank Pich Tantichukaitikul for the AMG program that was used to

construct the membrane model. We also thank the Large Scale Simulation Research Laboratory, National Electronics and Computer Technology Center (NECTEC), National Science and Technology Development Agency (NSTDA), Thailand, for computational resources. This work was partly supported by a grant from the National Center for Genetic Engineering and Biotechnology (BIOTEC), NSTDA, Thailand.

Author contributions

W.N., S.H. and M.R. designed the research in the manuscript. W.N. conducted the molecular dynamics simulations and analyzed the results. W.N. and M.R. wrote the manuscript and prepared all figures. All authors reviewed the manuscript.

Additional information

Supplementary information accompanies this paper at http://www.nature.com/scientificreports

Competing financial interests: The authors declare no competing financial interests.

How to cite this article: Nawae, W., Hannongbua, S. & Ruengjitchatchawalya, M. Defining the membrane disruption mechanism of kalata B1 via coarse-grained molecular dynamics simulations. *Sci. Rep.* **4**, 3933; DOI:10.1038/srep03933 (2014).